Buoyant-Thermocapillary Flow with Nonuniform Supra-Heating: II. Two-Phase Behavior

David N. Schiller* and William A. Sirignano†
University of California, Irvine, Irvine, California 92717

A computational study has been made of transient heat transfer and fluid flow in a cylindrical enclosure containing a two-layer gas-liquid system heated nonuniformly from above. The effects of gas-liquid phase coupling, variable density and thermophysical properties, and vaporization have been considered. At all gravity levels investigated (0–1 g_n), the presence of the gas has little effect on the liquid phase. Fuel vapor is transported more quickly to the heat source at higher gravity levels, which indicates that ignition delay should decrease with increasing gravity level. At reduced gravity, diffusion is dominant and surface tension significantly affects the flow pattern in the gas phase. The variation of density and thermal conductivity are important in the gas phase, whereas in the liquid phase, variable viscosity is most important.

Nomenclature

D_{ij} = D'_{ij}/D_*, binary diffusion coefficient
H' = height of gas or liquid phase
h_{fg} = latent heat of vaporization
M = molecular weight
P_G = P'_G/P_*, global pressure
P_{sat} = saturated vapor pressure
Y = mass fraction of species
Δt = time step

Subscripts
A = air
F = fuel vapor
g = gas phase
i = species index (e.g., air, fuel vapor)

Superscripts
$'$ = dimensional quantity

Standard symbols (ρ, μ, k, etc.) are used for fluid properties. Variables not defined in the above nomenclature are either defined in Part I of this paper, or are defined when first used in the text. Unless otherwise specified, a variable without a superscript or subscript represents a nondimensional quantity. All reference quantities are evaluated at 300 K, which is taken as the initial temperature of the fluid, T'_o.

Introduction

FIRE safety problems of ignition and flame spread above a pool of flammable liquid arise in many accident situations where a flammable liquid spills in the vicinity of a hot ignition source. Another prototypical hazard situation might be the rupture of a fuel tank when hot engine parts or exhaust gases may appear in close proximity of liquid fuel. Heat and mass transport which control ignition delay and flame spread rates are complicated by multiple energy and mass transport processes, phase change, and chemical reaction.

The literature of liquid pool burning theory has for the most part neglected the gas and liquid phase coupling, and concerned itself solely with liquid motion.[1,2] However, the most interesting scientific situation (and one of very practical importance) involves not-so-volatile fuels whereby the coupling between the liquid and gas phases is of critical importance. That is, heat from the gas phase is required to vaporize some portion of the liquid fuel in order to provide a combustible mixture in the gas phase. Convective heat and mass transport between the liquid and gas phases is critical and often dominant during the preignition period. Other modes of heat transfer, such as thermal radiation from the ignition source, may also play a very important role in the liquid heating. Temperature gradients in the gas and liquid phases, as well as concentration gradients in the gas mixture, create natural convection currents. Temperature gradients on the liquid surface initiate "surface-tension-driven convection" which can be a critical factor in the ignition delay and flame spread phenomena. On account of nonuniform heating from above due to the ignition source or the flame, liquid motion will be driven by both surface-tension gradients and by buoyancy. If only liquid motion were considered, then since these driving forces generally support in concert surface fluid motion away from the heat source, one would be led to believe that increasing either buoyancy or surface tension would delay ignition yet support flame spread (as the convection assists the preheating process ahead of the flame). However, results of Part I of this two-part paper[3] indicate that buoyancy and thermocapillarity are highly coupled with nonuniform supra-heating. Buoyancy stabilizes the hot subsurface liquid above the colder core fluid, thus preventing the thermocapillary-driven vortex from penetrating into the liquid volume. Therefore, for a given heat flux profile incident on the liquid surface, the liquid surface temperatures are greater at higher gravity levels, despite the fact that the liquid surface velocities are also greater. Since vaporization rates increase with increasing liquid temperature, increasing gravity could lead to *shorter* ignition delay and faster flame spread. This hypothesis, based solely on the uncoupled liquid behavior, may be altered when gas-phase heat and mass transport is considered. In the gas phase, buoyancy-driven convection opposes the surface-tension-driven motion.[4] Buoyant convection opposes conduction of heat to the liquid surface, yet assists transport of fuel vapor toward the heat source. In contrast, thermocapillary-driven circulation above the liquid surface assists conduction of heat to the liquid surface, but opposes diffusion of fuel vapor toward the heat source.

The effects of variable density and thermophysical properties on the flow will also be investigated. Variable density is important in the gas phase because during preignition heating, high-temperature gradients are expected near the ignition source. In such a situation, the use of the constant density

Received Aug. 3, 1990; revision received Dec. 6, 1990; accepted for publication Dec. 7, 1990.

*Research Assistant. Member AIAA.
†Professor of Mechanical and Aerospace Engineering. Fellow AIAA.

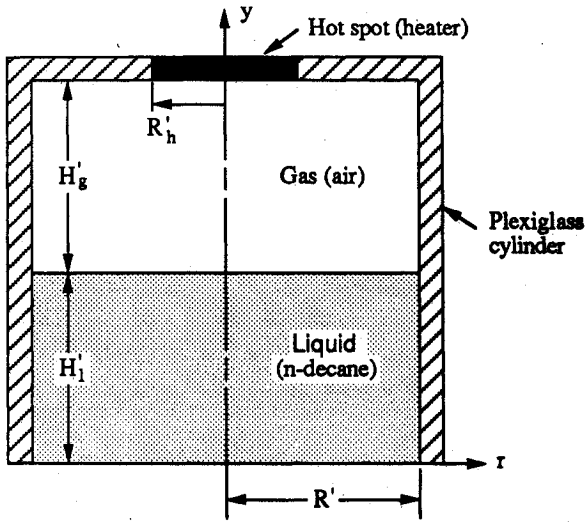

Fig. 1 Geometry of the problem. Part I of this two-part paper considered only the liquid phase with radiant heating from the heater.

approach along with the Boussinesq approximation may produce very serious quantitative errors in the analysis of the phenomena. The incorporation of variable thermophysical properties in the liquid phase is also important since the viscosity and volume expansion coefficient of many liquids vary considerably with temperature. Vaporization is included in the computational model in order to study the transport of fuel vapor in the gas phase.

The geometry of the problem is shown in Fig. 1. Here, the cylindrical enclosure of radius R' and height $H' = H'_g + H'_l$ contains a two-layer gas/liquid system. The initial temperature of the system is uniform at $T' = T'_o$. At $t = 0$, the temperature of a small circular spot (heater) of radius R'_h at the center of the top cover increases suddenly to $T' = T'_h >> T'_o$ and then remains constant. The total pressure in the gas phase is initially 1 atm. The initial condition for the mass fraction of fuel vapor in the gas phase is $Y_F(r, y, 0) = 0$. Unless otherwise specified, all results presented are for a 10 cm height and diameter plexiglass container (4-mm wall thickness) with $R'_h = 1$ cm, $T'_h = 800$ K or 1000 K, and $H'_g = 5$ cm.

Statement of the Problem

The mathematical formulation of the axisymmetric problem is based on the following assumptions:

1) The gas/liquid interface remains flat and horizontal at all gravity levels.[3] Recession of the liquid surface due to vaporization is neglected.

2) All surfaces are assumed opaque and black, and gas radiation is neglected. (Ref. 3 investigated the effects of volumetric absorption of radiation in the liquid.)

3) The "hot spot" has no thermal contact with the remaining part of the top cover (i.e., the side of the heater is insulated). The bottom of the liquid phase is maintained at the constant temperature $T' = T'_o$, while the side wall in the liquid phase is assumed adiabatic.

4) Chemical reactions are neglected.

5) The energy equation is simplified by the following approximations: (a) low Mach number flow, (b) work by body forces is neglected, (c) no volumetric heat sources, and (d) transport of energy by mass diffusion is neglected.

6) Solutocapillary forces are neglected since contamination by surfactants is not applicable.

Variable density and thermophysical properties were included in all simulations except for those used to test the effects of variable properties without vaporization. The nondimensional conservation equations are the same as in Part I with the following exceptions. In the gas phase, the conservation of species and energy are as follows

$$\frac{\partial}{\partial t}(\rho Y_i) + \frac{1}{r}\frac{\partial}{\partial r}\left[r\left(\rho u Y_i - \frac{\rho D_{ij}}{Sc_* Re_*}\frac{\partial Y_i}{\partial r}\right)\right] + \frac{\partial}{\partial y}\left(\rho v Y_i - \frac{\rho D_{ij}}{Sc_* Re_*}\frac{\partial Y_i}{\partial y}\right) = 0 \tag{1}$$

$$\frac{\partial(\rho h_1)}{\partial t} + \frac{1}{r}\frac{\partial}{\partial r}\left[r\left(\rho u h_1 - \frac{k/\bar{c}_p}{Pr_* Re_*}\frac{\partial h_1}{\partial r}\right)\right] + \frac{\partial}{\partial y}\left(\rho v h_1 - \frac{k/\bar{c}_p}{Pr_* Re_*}\frac{\partial h_1}{\partial y}\right) = \left(\frac{P}{\rho_g c_{p,g} T}\right)_* \left(\frac{\partial P_G}{\partial t}\right) \tag{2}$$

Physical properties (e.g., ρ, $\bar{c}_p$) for vapor-air mixtures are calculated using the standard additive rules for an ideal gas. Curve-fits for physical properties are given in Ref. 5.

In the v-momentum equation, the Boussinesq approximation (used only for the nonvaporizing case) may be obtained by replacing the last term, $g(1 - \rho)$, by $g(T - 1.0)$ for the gas phase and $g\beta_* T_*(T - 1.0)$ for the liquid phase (where T is evaluated at the center of the v-momentum finite difference control volume). For a constant property simulation, the physical properties of the liquid are calculated at $T' = T'_o$, while gas properties (unless otherwise specified) are evaluated at $T' = 0.5(T'_o + T'_h)$.

The dimensionless Reynolds, Schmidt, Prandtl, and Euler numbers are defined for each phase (with the exception of the Schmidt number) using reference quantities as follows: $Re_* = U_* L_* / \nu_*$, $Sc_* = \nu_*/D_*$, $Pr_* = \nu_*/\alpha_*$, and $Eu_* = (\Delta P)_*/\rho_* U_*^2$. Note that these numbers are constant, since they are defined with reference quantities evaluated at 300 K, although they differ between the gas and liquid phase. Since the properties are highly variable (especially density), there is some arbitrariness in the selection of the reference parameters. Reference parameters used in the computations were selected as follows: $L_* = R'$, $U_* = 1$ cm/s, and $t_* = L_*/U_*$.

The hydrodynamic boundary conditions are as follows: a) zero velocity on all solid walls ($u = v = 0$); b) symmetry of the velocity field at the axis ($u = 0$, $\partial v/\partial r = 0$ at $r = 0$); and c) balance of the stresses and mass flux and continuity of the radial velocity on the gas/liquid interface

$$\left(\frac{\partial u}{\partial y}\right)_l = \frac{\mu_{*,g}}{\mu_l \mu_{*,l}}\left[\left(\mu\frac{\partial u}{\partial y}\right)_g + \left(\frac{T_*}{\mu_{*,g} U_*}\right)\left(\frac{\partial \sigma'}{\partial T'}\right)_* \frac{dT_{lg}}{dr}\right] \tag{3}$$

$$u_g = u_l \tag{4}$$

$$v_g = -\frac{1}{Sc_* Re_*}\left[\left(\frac{D_{ij}}{1 - Y_{F,lg}}\right)\left(\frac{\partial Y_F}{\partial y}\right)_{lg}\right] \tag{5}$$

$$v_l = \frac{\rho_{*,g}\rho_g}{\rho_{*,l}\rho_l} v_g \tag{6}$$

Here v_g is the mass-average vaporization velocity based on the Stefan flow assumption.[6] The mass fraction of fuel vapor at the liquid surface, $Y_{F,lg}$, is determined by

$$Y_{F,lg} = \frac{\chi_{F,lg} M_F}{\chi_{F,lg} M_F + (1 - \chi_{F,lg}) M_A} \tag{7}$$

where

$$\chi_{F,lg} \simeq \frac{P'_{sat}(T'_{lg})}{P'_G} \tag{8}$$

When vaporization is not included in the analysis, the boundary condition becomes $v_g = v_l = 0$. A zero flux boundary condition for Y_F is used at the walls and along the centerline in the gas phase.

The thermal boundary conditions are as follows: a) constant temperature of the hot spot ($T = T_h$ at $r < R_h$, $y_g = H_g'/L_*$); b) constant temperature at the bottom of the liquid phase ($T = 1$ at $y_l = 0$); c) heat balance and continuity of the temperature on the gas/liquid interface

$$\left(\frac{\partial T}{\partial y}\right)_l = \frac{k_{*,g}}{k_l k_{*,l}}\left[\left(k\frac{\partial T}{\partial y}\right)_g + \frac{q_R'}{q_{g,*}} - \frac{\rho_g' v_g' h_{fg}'}{q_{g,*}}\right] \tag{9}$$

$$T_g = T_l \tag{10}$$

d) adiabatic side wall in the liquid phase ($\partial T_l/\partial r = 0$ at $r = 1, 0 < y < H_l'/L_*$); and e) transient heat conduction equation governing the two-dimensional temperature distribution in the side and top walls in the gas phase using constant properties for the walls

$$\frac{\partial T_w}{\partial t} = \frac{\alpha_w}{Pe_{*,w}}\left(\frac{\partial^2 T_w}{\partial r^2} + \frac{1}{r}\frac{\partial T_w}{\partial r} + \frac{\partial^2 T_w}{\partial y^2}\right) \tag{11}$$

Here $Pe_{*,w} = Pr_{*,w}Re_{*,w}$. For plexiglass, the properties used were[6]: $\rho_w' = 1185$ kg/m^3, $c_w' = 1470$ J/kg·K, and $k_w' = 0.21$ W/m·K. Shape factors used for radioactive heat transfer in the gas phase are given in Ref. 7.

Equation (11) is solved explicitly using the total heat fluxes from the gas phase from the beginning of the time step for the inner wall boundary condition and Newton's law of cooling for the outside wall boundary condition. The external heat transfer coefficient, $\bar{h}_{\text{conv}}'$, is taken as[8]

$$\bar{h}_{\text{conv}}' = \frac{k'}{L'}\left[0.678\, Ra^{1/4}\left(\frac{Pr}{0.952 + Pr}\right)^{1/4}\right] \tag{12}$$

where

$$Ra = \frac{g' L'^3(|T_{w,b}' - T_e'|/T_e')}{\nu'\alpha'} \tag{13}$$

is the Rayleigh number of the air and T_e' is the outside environment temperature (assumed 300 K). In Eqs. (12) and (13), properties are of air evaluated at $T' = 0.5(T_e' + T_{w,b}')$. Also, $T_{w,b}'$ is the boundary temperature of the wall and L' is the length of the wall. Although Eq. (12) is a correlation for vertical walls, it is also used in the present study for the external heat transfer for the top wall of the cylinder. Little error is introduced here as $\bar{h}_{\text{conv}}'$ is approximately 5 W/(m^2·K), which leads to external heat fluxes that are a full order of magnitude less than the total heat fluxes on the inner walls.

Method of Solution

Pressure Splitting

The total pressure (P') is divided into three parts in the computational model: global pressure (P_G'), dynamic pressure (P_D'), and the hydrostatic pressure ($\rho_* g_y' y' = -\rho_* g' y'$). Hence

$$P' = P_G'(t) + P_D'(r, y) - \rho_* g' y' \tag{14}$$

The global pressure (used only in the gas phase) is calculated as

$$P_G' = \frac{1}{V'}\int\int\int\left(\rho' T' \mathcal{R}' \sum_i Y_i/M_i'\right) dV' \tag{15}$$

where V' is the volume of the gas phase and $\mathcal{R}'$ is the universal gas constant. Since $P_G' \sim 10^5$ N/m^2 while

$$P_{D,\max}' \sim \rho_* |\vec{V}|_{\max}^2 \sim 10^{-2} \text{ N/m}^2$$

and

$$(\rho_* g' y')_{\max} \sim 1 \text{ N/m}^2$$

we can make the approximation $P' \simeq P_G'$. Thus, the global pressure is used to calculate density in the gas phase using the ideal gas law at each cell location. The global pressure increases during the heating and vaporization processes.

Numerical Method

The numerical method uses the SIMPLE algorithm[9] with the SIMPLEC modification[10] and the hybrid-differencing scheme. Gas and liquid properties are calculated at the beginning of the time step. Only values of c_p are updated during the iteration cycle of the SIMPLE algorithm. This helps stabilize the solution. Values of c_p are updated in order to update values of enthalpy. The gas-phase and liquid-phase solutions are phase-split in that the solution at time t represents the gas phase at time t and the liquid phase at time $t + \frac{1}{2}\Delta t$. The sequential calculation procedure for each time step is as follows:

1) Using values of the total heat flux (radiative plus conductive) to the walls in the gas phase at time t as a boundary condition, wall temperatures in the gas phase at time $t + \Delta t$ are calculated using an explicit scheme. These wall temperatures are then used as a boundary condition for the gas phase solution below.

2) Determine gas-phase solution at time $t + \Delta t$. Boundary values of wall temperatures (from explicit solution) and liquid temperatures and velocities (from time $t + \frac{1}{2}\Delta t$) are used [see Eqs. (4), (5) and (10)].

3) Determine liquid-phase solution at time $t + \frac{3}{2}\Delta t$. Boundary values of v_g and *gradients* of T_g and u_g (from time $t + \Delta t$) are used [see Eqs. (3), (6) and (9)].

The calculation procedure for a single-phase, gas-only simulation is similar to the above except that a relatively thick (1.2 cm), isothermal wall is used at the bottom of the gas phase. The convergence criteria used for the governing equations were discussed in Ref. 3 (the convergence criterion for the species equation is the same as that for the momentum and energy equations).

Based on results of a grid dependence study,[3] 42 grid points (40 uniformly spaced cells plus 2 columns of boundary node points) were used in the radial direction. In the axial direction, a mesh size of $\sim\frac{1}{3}$ mm or less was used for the first 5 mm below the liquid surface. Unless otherwise specified, in the liquid phase a total of 40 cells (42 grid points) were used in the axial direction for a pool depth of 5 cm (less cells were used for shallower pools). A nonuniform mesh with geometric progression was used after the first 5 mm below the liquid surface. A nonuniform mesh (42 grid points) was also used in the axial direction of the gas phase. A mesh size of ~1 mm was used for the first 5 mm below the top wall, while a 0.5 mm mesh was used for the first 5 mm above the liquid surface. Four cells were used for the 4 mm thickness of the top and side wall, with the cells aligned longitudinally with the cells from the adjacent gas-phase domain. Ten cells were used for the bottom of the gas phase in the single-phase (gas-only) simulations. The time step was typically 0.005–0.01 s and required approximately 0.5 s of CPU time on a CRAY Y-MP for a 42 × 42 grid in each phase.

Results and Discussion

The flow field in the enclosure is presented in terms of the streamlines and the fluid velocities and temperatures. In polar

coordinates, the nondimensional quasi-steady stream function $\psi(r, y)$, used here only for graphical purposes,[3] is defined by

$$\psi = -\int_0^r \rho r v dr, \qquad \psi = r\int_0^y \rho u dy \tag{16}$$

where $\psi = 0$ at $r = 0, y = 0$. Unless otherwise specified, all results will be shown for $t' = 100$ s. At this time, the flow reaches a quasi-steady state, characterized by stabilized boundary layers and vortical structures whose shapes remain essentially constant.

The computer code was tested successfully in three ways: a) a single-phase, constant property, planar geometry comparison with the benchmark solution of De Vahl Davis and Jones,[11] b) comparisons with experimental results for heating from above with both single-phase (air-only) and two-phase (with silicone oil) configurations,[12] and c) constant-property comparisons with numerical results obtained with a modified SMAC method.[7] Details of these comparisons are given in Refs. 12 and 13. Silicone oil was used for the comparison with experiments because of its well-known properties and its resistance to surface contamination.[14]

Effects of Gas-Liquid Coupling

As shown in Figs. 2 and 3, at all gravity levels investigated, the radiative heat flux to the liquid surface is much greater than the conductive flux and the enthalpy flux, and the gas shear is negligible compared to the surface-tension stress. Therefore, the presence of the gas phase has very little effect on the liquid behavior. The isotherm contours in the liquid phase are similar to the previous liquid-only study[3]: the subsurface isotherms are flat at 1 g_n, which leads to larger surface temperature gradients (due to the nonuniform supra-heating) and thus larger velocities on the liquid surface compared to reduced gravity simulations. At reduced gravity, warmed su-

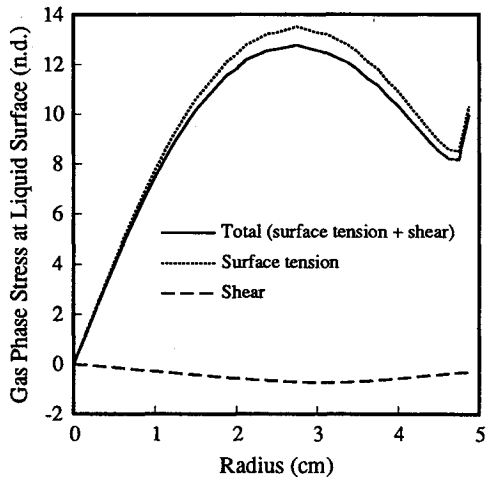

a) 1 g_n

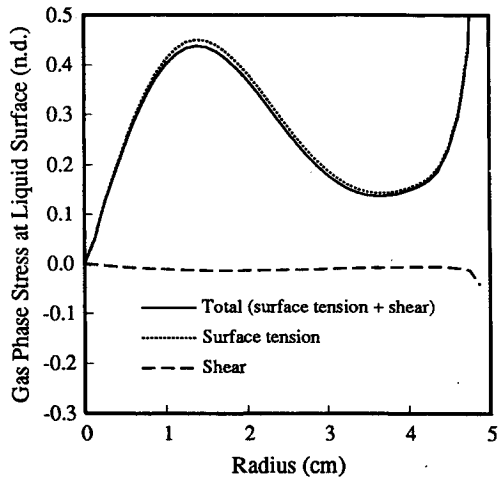

b) 10^{-4} g_n

Fig. 2 Components of the stress at the liquid surface due to surface tension and gas-phase shear at a) 1 g_n and b) 10^{-4} g_n ($t' = 100$ s).

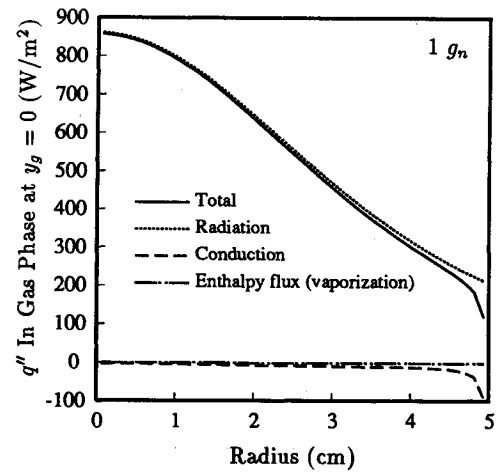

Fig. 3 Components of the heat flux at the liquid surface due to radiation, gas-phase conduction, and vaporization ($t' = 100$ s). The heat flux toward the surface is shown as positive. Reduced gravity results are nearly identical to the above 1 g_n plot.

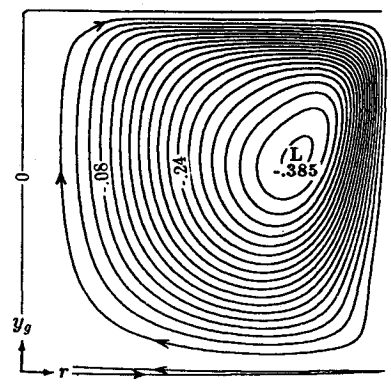

a) 1 g_n

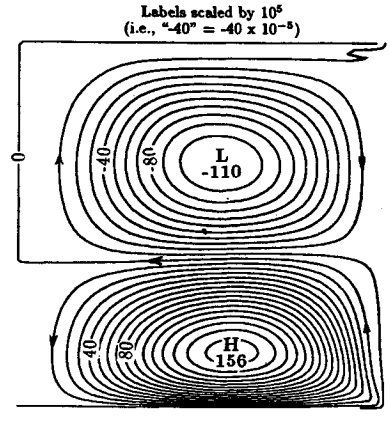

b) 10^{-4} g_n

Fig. 4 Nondimensional stream function contours in the gas phase at a) 1 g_n and b) 10^{-4} g_n. The left side of each plot corresponds to the axis of symmetry of the cylinder.

Table 1 Liquid surface data from two-phase simulations (800 K heater)

Run No.	g'/g_n	H_l'/R'	$T'_{lg,\max}$ [K]	$(\Delta T)'_{lg}$ [K]	Ma	$U'_{lg,avg}$ [mm/s]	$\overline{Re_l}$
1.	1	1	310.19	0.8285	5.68×10^4	1.489	69.19
2.	1	1/4	310.19	0.8300	5.69×10^4	1.492	69.33
3.	1	1/10	310.05	0.8201	5.62×10^4	1.426	66.26
4.	1	1/20	308.02	0.9441	6.47×10^4	1.477	68.63
5.	10^{-2}	1	308.69	0.0958	6.57×10^3	0.443	20.59
6.	10^{-2}	1/4	308.79	0.0956	6.56×10^3	0.434	20.17
7.	10^{-2}	1/10	309.17	0.1990	1.36×10^4	0.643	29.88
8.	10^{-2}	1/20	307.89	0.8175	5.61×10^4	1.393	64.73
9.	10^{-4}	1	308.36	0.0256	1.76×10^3	0.303	14.08
10.	10^{-4}	1/4	308.64	0.0536	3.68×10^3	0.360	16.73
11.	10^{-4}	1/10	309.28	0.1935	1.33×10^4	0.652	30.30
12.	10^{-4}	1/20	308.05	0.8466	5.81×10^4	1.445	67.15
13.	0	1	308.37	0.0245	1.68×10^3	0.301	13.99

Table 2 Maximum and minimum values of stream function from two-phase and gas-only simulations (800 K heater)

Run No.	g'/g_n	H_l'/R'	$\psi_{g,\max}$	@ r_g, y_g	$-\psi_{g,\min}$	@ r_g, y_g	$-\psi_{l,\min}$	@ r_l, y_l
Two-Phase Results								
1.	1	1	2.22×10^{-4}	0.45, 0.01	3.85×10^{-1}	0.75, 0.60	9.78×10^{-4}	0.73, 0.980
2.	1	1/4	2.23×10^{-4}	0.45, 0.01	3.85×10^{-1}	0.75, 0.60	9.79×10^{-4}	0.73, 0.230
3.	1	1/10	2.01×10^{-4}	0.45, 0.01	3.82×10^{-1}	0.75, 0.60	9.05×10^{-4}	0.73, 0.080
4.	1	1/20	7.60×10^{-4}	0.70, 0.01	3.44×10^{-1}	0.78, 0.69	8.92×10^{-4}	0.70, 0.035
5.	10^{-2}	1	6.56×10^{-4}	0.75, 0.04	5.38×10^{-2}	0.60, 0.69	7.37×10^{-4}	0.70, 0.953
6.	10^{-2}	1/4	6.09×10^{-4}	0.78, 0.04	5.37×10^{-2}	0.60, 0.69	7.14×10^{-4}	0.68, 0.203
7.	10^{-2}	1/10	1.25×10^{-3}	0.73, 0.05	5.39×10^{-2}	0.60, 0.69	7.73×10^{-4}	0.70, 0.067
8.	10^{-2}	1/20	4.81×10^{-3}	0.70, 0.08	5.21×10^{-2}	0.60, 0.69	9.01×10^{-4}	0.70, 0.035
9.	10^{-4}	1	1.56×10^{-3}	0.58, 0.16	1.10×10^{-3}	0.55, 0.69	2.33×10^{-3}	0.60, 0.779
10.	10^{-4}	1/4	1.92×10^{-3}	0.60, 0.16	1.03×10^{-3}	0.55, 0.69	1.02×10^{-3}	0.63, 0.170
11.	10^{-4}	1/10	3.95×10^{-3}	0.65, 0.17	6.85×10^{-4}	0.50, 0.73	8.06×10^{-4}	0.70, 0.067
12.	10^{-4}	1/20	9.66×10^{-3}	0.65, 0.17	2.07×10^{-4}	0.38, 0.82	9.35×10^{-4}	0.70, 0.035
13.	0	1	2.08×10^{-3}	0.58, 0.22	1.14×10^{-4}	1.00, 0.00	2.39×10^{-3}	0.60, 0.779

Gas-Only Results

Run No.	g'/g_n	$\psi_{g,\max}$	@ r_g, y_g	$-\psi_{g,\min}$	@ r_g, y_g
1.	1	0	0, 0	3.58×10^{-1}	0.78, 0.67
5.	10^{-2}	2.48×10^{-6}	0.98, 0.98	5.72×10^{-2}	0.60, 0.67
9.	10^{-4}	9.45×10^{-6}	0.70, 0.98	1.79×10^{-3}	0.55, 0.57

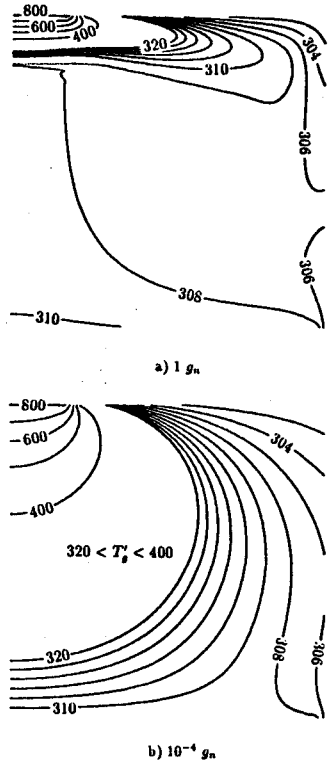

Fig. 5 Isotherm contours in the gas phase at a) 1 g_n and b) 10^{-4} g_n.

pra-heated surface fluid recirculates downwards near the side wall. Therefore, at a given height below the liquid surface, the temperature increases with increasing radius. This leads to smaller liquid surface temperature gradients, since the supra-heating is nonuniform, and smaller liquid surface velocities due to Marangoni convection. Table 1 shows that, consistent with the liquid-only results: a) for shallow pools (viscous flow), the liquid surface temperature and velocity profiles are insensitive to gravity level and b) for deep pools (depths greater than the subsurface vortex height, i.e., boundary layer flow), T_{lg} and U_{lg} are insensitive to H_l'.

In the gas phase, two primary vortices are generally formed (Fig. 4): a clockwise rotating vortex below the heater (driven by buoyancy) and a counterclockwise rotating vortex immediately above the liquid surface (driven by the liquid surface motion). The surface-tension-driven cell in the gas phase was predicted numerically by Furuta,[4] and was theorized by Sirignano[15] and Glassman[16] to play an important role in flame spread over liquid fuels. The present study shows that, at 1 g_n, the buoyancy-driven cell dominates the flow in the gas, while the height of the surface-tension-driven cell is $O(1\text{ mm})$. As the gravity level is reduced, the strength and height of the surface-tension-driven vortex increases relative to the buoyancy-driven cell, until at zero gravity, one counterclockwise rotating vortex fills the gas phase.

Table 2 summarizes the strength and location of the vortex centers for various gravity levels and liquid pool heights. Comparison with gas-only results shows that the surface-tension-driven cell has very little effect (less than 10%) on the strength of the buoyancy-driven vortex in the gas for $g' \geq 10^{-2}$ g_n,

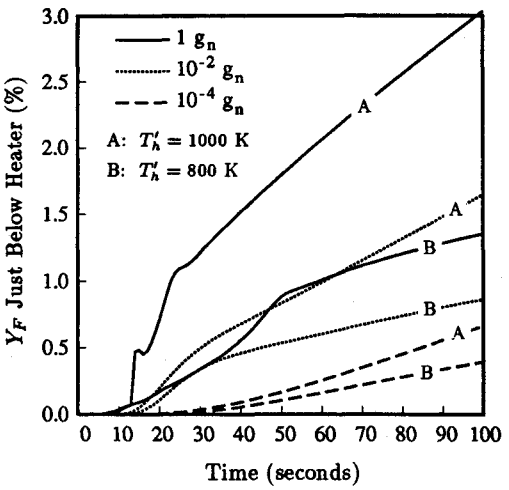

Fig. 6 Mass fraction of fuel vapor (Y_F) just below heater (r' = 4 mm, $H'_g - y'_g$ = 2.5 mm) as a function of time for different gravity levels and heater temperatures.

while at 10^{-4} g_n the difference is ~60%. Note that, for 10^{-4} to 1 g_n, one clockwise rotating vortex filled the majority of the gas phase in the gas-only simulations. Figure 5 shows isotherm contours in the gas phase at 1 g_n and at 10^{-4} g_n (from two-phase simulations). At 1 g_n, natural convection forces the hot isotherms to remain within ~1 cm of the heater, while at 10^{-4} g_n conduction is clearly dominant.

Vaporization Effects

Over the investigated range, including vaporization in the above variable property simulations did not significantly change the temperature or radial velocities in the gas or liquid phase. Area-weighted average vaporization velocities, $\bar{v}'_g$ at $y_g = 0$, are O (5–15 μm/s) and increase with increasing gravity level. These velocities are 2–4 orders of magnitude less than the velocities in the bulk of the gas phase.

Since liquid surface temperatures are greater at higher gravity levels, the mass fraction of fuel vapor near the liquid surface is also greater. Moreover, at 1 g_n, buoyancy-driven-convection transports the fuel vapor quickly toward the heat source, whereas at reduced gravity levels the transport of vapor toward the heater is slower since the surface-tension-driven convection opposes the diffusion of fuel vapor (see Figs. 6 and 7). Since the reaction rate is linearly dependent on Y_F and exponentially dependent on T_g, results from the present study indicate that increasing the gravity level should decrease ignition delay. This is consistent with the results of a related open pool study,[5] in which a small hot spot was placed 1–4 mm above the liquid surface. Figure 7a shows that, at 1 g_n, the mass fraction of fuel vapor immediately above the liquid surface reaches the lean flammability limit of n-decane in air (which is cited as 0.033–0.038 by Coward and Jones).[17] However, it is erroneous to imply that ignition will occur at this point since the maximum reaction rate is expected to be near the heater due to the exponential dependence of reaction rate on temperature. The effects of finite-rate chemical kinetics must be included in the analysis to predict quantitatively the ignition delay.

Variable Property Effects

Four simulations were used for this comparison: a) constant properties with the Boussinesq approximation (gas properties evaluated at T'_o), b) constant properties [gas properties evaluated at $0.5(T'_o + T'_h)$], c) variable density (no Boussinesq approximation) with the other properties (μ, c_p, and k) held constant [gas properties taken at $0.5(T'_o + T'_h)$], and d) all properties variable. Each case did not include the effects of vaporization. As shown by Table 3, the constant property assumption with the Boussinesq approximation significantly

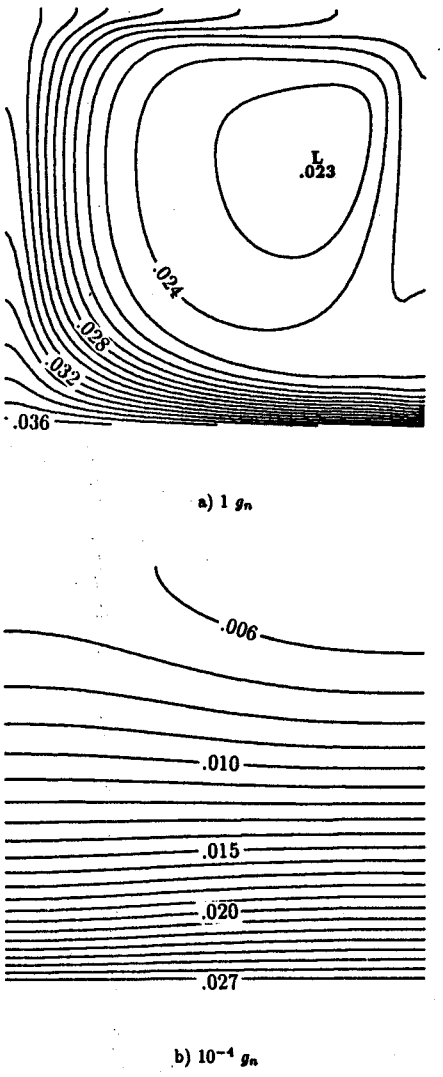

Fig. 7 Mass fraction of fuel vapor contours at a) 1 g_n and b) 10^{-4} g_n (T'_h = 1000 K).

underpredicts gas temperatures immediately below the heater, overpredicts velocities in the majority of the gas phase, and underpredicts liquid surface velocities. Variable density and thermal conductivity are important in the gas phase, whereas in the liquid phase, variable viscosity is most important.

In the gas phase, evaluating constant properties at T'_o rather than $0.5(T'_o + T'_h)$ resulted in a poorer prediction of the temperature field near the heater, but a better prediction of the velocity field in the gas phase at normal gravity. This is because the volume-averaged temperature in the gas phase is ~310–320 K at 1 g_n, as convection causes the hot isotherms to remain close to the heater. The average density of the fluid, which is inversely proportional to this temperature, is related to the inertia of the fluid (i.e., the fluid's resistance to a buoyant driving force). Although evaluating the density at 550 K or 650 K everywhere in the gas phase is more accurate close to the heater, the buoyant driving force acts over a large characteristic length (on the order of the radius of the cylinder), and hence, the underprediction of the average density results in an overprediction of the velocities in the gas phase.

The importance of variable viscosity in the liquid is consistent with the results of Napolitano et al.,[18] who showed that for Marangoni convection in a cylindrical floating zone geometry, higher liquid velocities are calculated with variable viscosity. Comparison of properties of liquid n-decane shows that, as expected, viscosity varies more with temperature than does either thermal conductivity, heat capacity, or density.

Table 3 Effects of variable properties (no vaporization), $t' = 100$ s

g'/g_n	T'_h [K]	IPROP[b]	$T'_{lg,max}$ [K]	$(\Delta T)'_{lg}$ [K]	$U'_{lg,max}$ [mm/s]	$U'_{g,max}$ [cm/s]	$V'_{g,max}$ [cm/s]	$T'_g(0, 0.95)$[a] [K]
1	800	3	310.19	0.8285	1.955	5.97	4.05	535.3
1	800	2	310.04	0.9287	1.885	5.47	4.53	496.6
1	800	1	310.06	0.9379	1.871	8.02	6.40	483.2
1	800	0	310.12	0.8632	1.812	5.25	5.54	394.6
1	1000	3	324.56	1.266	3.005	7.80	7.19	628.9
1	1000	2	323.83	1.642	2.881	7.11	7.61	559.0
1	1000	1	323.83	1.654	2.742	10.79	11.72	546.8
1	1000	0	324.26	1.475	2.516	7.86	10.50	407.6
10^{-4}	1000	3	320.50	0.0248	0.5040	0.050	0.029	882.8
10^{-4}	1000	2	319.46	0.0331	0.5312	0.053	0.013	836.4
10^{-4}	1000	1	319.39	0.0327	0.5281	0.053	0.024	836.3
10^{-4}	1000	0	320.04	0.0264	0.4632	0.046	0.043	831.2

[a]Temperature in gas phase at $r = 0$, $y = 0.95$.
[b]3, variable properties; 2, variable-density-only; 1, constant properties [gas properties evaluated at $0.5(T'_o + T'_h)$]; 0, constant properties (gas properties evaluated at T'_o).

Conclusions

A computational study was made of the transient heat transfer and fluid flow in a cylindrical enclosure containing a two-layer gas-and-liquid system heated nonuniformly from above. At all gravity levels investigated (0–1 g_n), the radiative heat flux to the liquid surface is much greater than the conductive flux and the enthalpy flux, and the gas shear is negligible compared to the surface-tension stress. Therefore, the presence of the gas phase has very little effect on the liquid behavior for the configuration studied. Conversely, at reduced gravity levels surface tension significantly affects the flow pattern in the gas phase. Surface-tension-driven convection opposes the diffusion of fuel vapor at reduced gravity, causing transport of fuel vapor toward the heat source to be much slower than at normal gravity. Since the reaction rate is linearly dependent on Y_F and exponentially dependent on T_g, this suggests that ignition delay should decrease with increasing gravity level. The constant property assumption with the Boussinesq approximation significantly underpredicts gas temperatures immediately below the heater, overpredicts velocities in the majority of the gas phase, and underpredicts liquid surface velocities. Variable density and thermal conductivity are important in the gas phase, whereas in the liquid phase, variable viscosity is most important. The detailed geometry of the problem does not modify the conclusions about the coupling between buoyancy and surface tension, the transport of fuel vapor in the gas phase, or the effects of variable properties. Ignition delay will be affected by these behaviors for most scenarios of liquid pool fires.

Appendix: Small-Time Solutions for T'_{lg} and U'_{lg}

As was done by Abramzon et al.,[7] small-time analytical solutions were used for the temperature of the liquid surface and inner walls of the gas phase, and for the liquid surface radial velocity. This was necessary because the values for these boundary conditions, when derived from Eqs. (3) and (9) (with an analogous boundary condition equation for the inner walls), are not an explicit function of time. Therefore, when radiation is included in the analysis, initially unrealistic values will be calculated. For the liquid surface, the analytical solutions are[7]

$$T'_{lg}(t) \simeq T'_o + 2\frac{q'_R}{k_{*,l}}\sqrt{\frac{\alpha_{*,l}t'}{\pi}} \tag{A1}$$

$$u'_{lg} \simeq \frac{\sigma'_T}{2\rho_{*,l}k_{*,l}\sqrt{Pr_{*,l}}}\left(\frac{dq'_R}{dr'}\right)t' \tag{A2}$$

where $\sigma'_T = (\partial\sigma'/\partial T')_* = -9.2 \times 10^{-5}$ N/m·K for liquid n-decane. The analytical solutions given by Eqs. (A1) and (A2) are used only for $t' < 0.25$ s and $t' < 0.18$ s, respectively. For a given mesh size immediately below the liquid surface, at these "cutoff" times the analytical solutions correspond to the solutions found from the boundary conditions.

Acknowledgments

Research at the University of California at Irvine was conducted in support of NASA Grant NAG 3-627 under the technical monitoring of Howard Ross (NASA-LeRC). The computational research was supported in part by the San Diego Supercomputer Center through an allocation of computer time. The authors are grateful to Howard Ross for his experimental support and technical discussions. We are indebted to Boris Abramzon who wrote the original algorithm of our computer code and several of the subroutines.

References

[1]Torrance, K. E., "Subsurface Flows Preceding Flame Spread Over a Liquid Fuel," *Combustion Science and Technology*, Vol. 3, 1971, pp. 113–143.

[2]Torrance, K. E., and Mahajan, R. L., "Surface Tension Flows Induced by a Moving Thermal Source," *Combustion Science and Technology*, Vol. 10, 1975, pp. 125–136.

[3]Schiller, D. N., and Sirignano, W. A., "Buoyant-Thermocapillary Flow with Nonuniform Supra-Heating: I. Liquid Phase Behavior," *Journal of Thermophysics and Heat Transfer*, Vol. 6, No. 1, 1992, pp. 105–112.

[4]Furuta, M., Humphrey, J. A. C., and Fernandez-Pello, A. C., "Prediction of Flame Spread Hydrodynamics Over Liquid Fuel," *PhysicoChemical Hydrodynamics*, Vol. 6, No. 4, 1985, pp. 347–372.

[5]Schiller, D. N., and Sirignano, W. A., 1991, "Ignition Delay of a Gas Mixture Above a Liquid Fuel Pool," presented at the *29th AIAA Aerospace Sciences Meeting*, Reno, NV, January 1991, Paper 91-0717.

[6]Edwards, D. K., Denny, V. E., and Mills, A. F., *Transfer Processes: An Introduction to Diffusion, Convection, and Radiation*, Hemisphere, New York, 1979.

[7]Abramzon, B., Edwards, D. K., and Sirignano, W. A., "Transient, Stratified, Enclosed Gas and Liquid Behavior with Concentrated Heating from Above," *Journal of Thermophysics and Heat Transfer*, Vol. 1, No. 4, 1987, pp. 355–364.

[8]Lienhard, J. H., *A Heat Transfer Textbook*, Prentice-Hall, Inglewood Cliffs, NJ, 1981.

[9]Patankar, S. V., *Numerical Heat Transfer and Fluid Flow*, McGraw-Hill, New York, 1980.

[10]Van Doormaal, J. P., and Raithby, G. D., "Enhancements of the SIMPLE Method for Predicting Incompressible Fluid Flows," *Numerical Heat Transfer*, Vol. 7, 1984, pp. 147–163.

[11]De Vahl Davis, G., and Jones, I. P., "Natural Convection in a Square Cavity: A Comparison Exercise," *Numerical Methods in Thermal Problems*, edited by R. W. Lewis et al., Pineridge Press, Swansea, Wales, 1981, pp. 553–572.

[12]Ross, H. D., Schiller, D. N., Disimile, P., and Sirignano, W.

A., "Behavior in Normal and Reduced Gravity of an Enclosed Liquid/Gas System with Nonuniform Heating From Above," presented at the 27th AIAA Aerospace Sciences Meeting, Reno, NV, January 1989, Paper 89-0070.

[13]Schiller, D. N., Abramzon, B., and Sirignano, W. A., "Enclosed Liquid/Gas System Heated Nonuniformly from Above: Variable Properties and Vaporization Effects," presented at the 26th ASME/AIChE National Heat Transfer Conference, Philadelphia; HTD-Vol. 106, *Heat Transfer Phenomena in Radiation, Combustion, and Fires*, edited by R. K. Shah, American Society of Mechanical Engineers, N.Y., 1989, pp. 389–398.

[14]Keller, J. R., and Bergman, T. L., "Thermocapillary Cavity Convection in Wetting and Nonwetting Liquids," *Numerical Heat Transfer*, Part A, Vol. 18, 1990, pp. 33–49.

[15]Sirignano, W. A., "A Critical Discussion of Theories of Flame Spread Across Solid and Liquid Fuels," *Combustion Science and Technology*, Vol. 6, 1972, pp. 95–105.

[16]Glassman, I., and Dryer, F. L., "Flame Spread Across Liquid Fuels," *Fire Safety Journal*, Vol. 3, 1980/1981, pp. 123–138.

[17]Coward, H. F., and Jones, G. W., "Limits of Flammability of Gases and Vapors," Bureau of Mines, Bulletin 503, 1952.

[18]Napolitano, L. G., Golia, C., and Viviani, A., "Effects of Variable Transport Properties on Thermal Marangoni Flows," *Acta Astronautica*, Vol. 13, No. 11/12, 1986, pp. 661–667.